

Strange metal and superconductor in the two-dimensional Yukawa-Sachdev-Ye-Kitaev model

Chenyuan Li,¹ Davide Valentini,^{2,3} Aavishkar A. Patel,⁴
Haoyu Guo,⁵ Jörg Schmalian,^{2,3} Subir Sachdev,¹ and Ilya Esterlis⁶

¹*Department of Physics, Harvard University, Cambridge MA 02138, USA*

²*Institut für Quantenmaterialien und Technologien,
Karlsruher Institut für Technologie, 76131 Karlsruhe, Germany*

³*Institut für Theorie der Kondensierten Materie,
Karlsruher Institut für Technologie, 76131 Karlsruhe, Germany*

⁴*Center for Computational Quantum Physics, Flatiron Institute, New York, New York, 10010, USA*

⁵*Laboratory of Atomic and Solid State Physics, Cornell University,
142 Sciences Drive, Ithaca NY 14853-2501, USA*

⁶*Department of Physics, University of Wisconsin-Madison, Madison, Wisconsin 53706, USA*

(Dated: June 21, 2024)

The two-dimensional Yukawa-Sachdev-Ye-Kitaev (2d-YSYK) model provides a universal theory of quantum phase transitions in metals in the presence of quenched random spatial fluctuations in the local position of the quantum critical point. It has a Fermi surface coupled to a scalar field by spatially random Yukawa interactions. We present full numerical solutions of a self-consistent disorder averaged analysis of the 2d-YSYK model in both the normal and superconducting states, obtaining electronic spectral functions, frequency-dependent conductivity, and superfluid stiffness. Our results reproduce key aspects of observations in the cuprates as analyzed by Michon *et al.* (Nat. Comm. **14**, 3033 (2023)). We also find a regime of increasing zero temperature superfluid stiffness with decreasing superconducting critical temperature, as is observed in bulk cuprates.

Higher temperature superconductors of correlated electron materials all display a ‘strange metal’ phase above the critical temperature for superconductivity [1, 2]. This is a metallic phase of matter where the Landau quasiparticle approach breaks down. It is characterized most famously by a linear in temperature (T) electrical resistivity. We use the term strange metal only for those metals whose resistivity is smaller than the quantum unit (h/e^2 in $d = 2$ spatial dimensions). Metals with a linear-in- T resistivity which is larger than the quantum unit are ‘bad metals’.

An often quoted model for a strange or bad metal (*e.g.* [3, 4]) is one in which there is a large density of states of low energy bosonic excitations, usually phonons, and then quasi-elastic scattering of the electrons off the bosons leads to linear-in- T resistivity from the Bose occupation function when T is larger than the typical boson energy. However, studies of the optical conductivity in the strange metal of the cuprates [5] show that the dominant scattering is inelastic, not quasi-elastic, and leads to a non-Drude power-law-in-frequency tail in the optical conductivity. The optical conductivity data has been incisively analyzed recently by Michon *et al.* [6]: they have shown that while the transport scattering rate (related to the real part of the inverse optical conductivity) exhibits Planckian scaling behavior [1], there are significant

logarithmic deviations from scaling in the frequency and temperature dependent effective transport mass (related to the imaginary part of the inverse optical conductivity). Furthermore, the optical conductivity data connects consistently with d.c. measurements of resistivity and thermodynamics.

Our paper presents a self-consistent, disorder-averaged analysis of a two-dimensional Yukawa-Sachdev-Ye-Kitaev (2d-YSYK) model, which has a spatially random Yukawa coupling between fermions, ψ , with a Fermi surface and a nearly-critical scalar field, ϕ . We use methods similar to those which yield the exact solution of the zero-dimensional Sachdev-Ye-Kitaev model. Such a 2d-YSYK model has been argued [7–9] to provide a universal description of quantum phase transitions in metals, associated with the condensation of ϕ , in the presence of impurity-induced ‘Harris’ disorder [10–12] with spatial fluctuations in the local position of the quantum critical point. We find results that display all the key characteristics of the optical conductivity and d.c. resistivity described by Michon *et al.*, as shown in Fig. 3.

Moreover, YSYK models also display instabilities of the strange metal to superconductivity [13–17], with the pairing type dependent upon the particular quantum phase transition being studied. We will examine an instability to spin-singlet pairing in a simplified model which

ignores the gap variation around the Fermi surface, and will therefore only apply to the anti-nodal regions of the cuprates. We present the evolution of the electron spectral function and superfluid density for $T < T_c$, the superconducting critical temperature. We find that the 2d-YSYK model exhibits a number of experimentally observed trends:

(i) It obeys the connection between scattering and pairing discussed by Taillefer [18], with a monotonic relation between T_c and the slope of the linear- T resistivity (Fig. 2b).

(ii) It has an overdoped regime where decreasing T_c is accompanied by an increasing $T = 0$ superfluid density (Fig. 5a), as is observed in bulk samples of the cuprates [19]. Our interpretation is that the opening of a gap for the fermions ψ in the superconducting state weakens the pairing interaction mediated by ϕ in a fully self-consistent theory at strong coupling [16, 17].

(iii) We study the relationship between the $T = 0$ superfluid density and the normal state conductivity at T_c , and find a connection similar to Homes' Law [20] (Figs. 5b and S12 in the supplement [21]).

The 2d-YSYK Model—Several works [22–29] have argued that clean quantum critical metals cannot serve as a universal model for transport in a strange metal, and that impurity-induced spatial disorder is essential. As a characteristic example, we therefore add Harris disorder to the Hertz-Millis theory of a quantum phase transition in a metal associated with an Ising-nematic order parameter ϕ [30]. Such disorder is provided by quenched random terms which preserve the Ising symmetry [24, 25]. Other order parameters, including those at non-zero wavevector, and Fermi-volume changing transitions without broken symmetries [31], also map to essentially the same 2d-YSYK model [7]. We define the 2d-YSYK model here as the Harris-disordered Hertz-Millis Lagrangian for ϕ and fermions ψ with dispersion $\varepsilon(\mathbf{k})$ [7, 27, 29, 32–34]:

$$\begin{aligned} \mathcal{L}_{2d\text{-YSYK}} = & \psi_\sigma^\dagger [\partial_\tau + \varepsilon(i\nabla) - \mu] \psi_\sigma + v(\mathbf{r}) \psi_\sigma^\dagger \psi_\sigma \\ & + \frac{1}{2} [(\partial_\tau \phi)^2 + c^2 (\nabla \phi)^2 + s \phi^2] + u \phi^4 \\ & + [g + g'(\mathbf{r})] \phi_\sigma \psi_\sigma^\dagger \mathcal{D}_\mathbf{r} \psi_\sigma. \end{aligned} \quad (1)$$

Here τ is imaginary time, we set $\hbar = 1$, s is the tuning parameter across the transition, u is a scalar self-interaction. The operator $\mathcal{D}_\mathbf{r} = \partial_x^2 - \partial_y^2$ is special to the Ising-nematic case, and will be set to unity for simplicity in our computations as it is unimportant apart from ‘cold spots’ on the Fermi surface. In order to obtain a spin-singlet superconductor we have spinful fermions, with σ the spin index.

$\mathcal{L}_{2d\text{-YSYK}}$ contains the two sources of disorder. One is the potential $v(\mathbf{r})$ acting on the fermions:

- **Spatially random potential** $v(\mathbf{r})$ with $\overline{v(\mathbf{r})} = 0$, $\overline{v(\mathbf{r})v(\mathbf{r}')} = v^2 \delta(\mathbf{r} - \mathbf{r}')$.

Its influence is familiar from the theory of weakly disordered metals [35], leading to marginally relevant localization effects on the fermions [35]. Much more relevant is the Harris disorder, which we have taken in the form of a spatially random Yukawa coupling $g'(\mathbf{r})$ adding to the spatially uniform Yukawa coupling g , and obeying

$$\overline{g'(\mathbf{r})} = 0, \quad \overline{g'(\mathbf{r})g'(\mathbf{r}')} = g'^2 \delta(\mathbf{r} - \mathbf{r}'). \quad (2)$$

By rescaling ϕ , it is possible to transform $g'(\mathbf{r})$ into a more familiar ‘random mass’ form of the Harris disorder, $s \rightarrow s + \delta s(\mathbf{r})$ [7]. Both forms of the disorder have been examined in earlier work, random $g'(\mathbf{r})$ [7, 9] and random $\delta s(\mathbf{r})$ [8], and similar results were obtained. We choose to work in the random $g'(\mathbf{r})$ formulation because it enables direct extension of methods employed for the exact solution of the zero-dimensional YSYK model [13–15, 36–41]. We restrict our analysis here to the simpler case with $g = 0$ for then the self-energies are functions of frequency alone; earlier work [7] has shown that perturbative corrections in g cancel in the transport response, partially justifying the $g = 0$ choice.

Two distinct regimes of behavior of $\mathcal{L}_{2d\text{-YSYK}}$ have been identified [8, 9]:

(i) There is a significant intermediate energy regime where the bosonic and fermionic eigenmodes are spatially extended. In this regime, the physics is self-averaging, and numerical results are consistent with the averaged Green’s function methods which yield the exact solution of the zero-dimensional YSYK model. This is the regime we address in the present paper by standard SYK methods.

(ii) At low T there is a crossover to a regime where bosonic eigenmodes are localized, while the fermionic eigenmodes remain extended [42]. Here, we must treat the disorder in the bosonic sector carefully: by a strong disorder renormalization [12], numerically exactly [8, 9], or map to ‘two-level system’ models [43, 44]. Recent analyses [45, 46] of $v(\mathbf{r})$ disorder effects along the lines of Ref. 35 near quantum criticality found singular corrections to the boson propagator, which we view as a precursor to boson localization. This boson localization regime is not described in the present paper.

Normal State Results—As we describe in the supplement [21], the self-consistent equations for the Green’s functions can be obtained by endowing the fields with flavor indices, and making the Yukawa coupling also random in flavor space. After a disorder average, and in the limit of a large number of flavors, we obtain the SYK-type equations which are indicated schematically in Fig. 1. We have solved the integral equations defined by the diagrams in Fig. 1 numerically on a 2D square lattice with nearest-neighbor hopping t and with fermion chemical potential $\mu = -0.5t$. The bosonic dispersion is chosen such that boson and fermion velocities are comparable $c \sim v_F$. These parameters are chosen to represent the generic properties of our model. In the main text

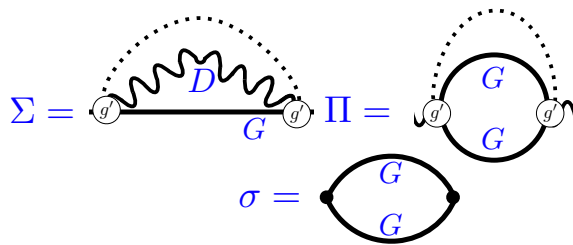


FIG. 1: Feynman diagrams for the ψ self energy Σ , and the ϕ self energy Π . The wavy line is the ϕ Green's function, and the smooth line is the ψ Green's function. All Green's functions include self energy corrections.

The dashed line represents an average over spatial disorder. All Green's functions and self energies become 2×2 matrices in the superconducting phase.

we primarily focus on results for two values of the interaction strength, $g' = 2t^{3/2}$ and $g' = 5t^{3/2}$, which are representative weak coupling (interacting energy smaller than the fermion bandwidth) and strong coupling (interacting energy larger than the fermion bandwidth) values, respectively. In the main text we focus on the case with no external impurity potential, $v = 0$. Further details describing the numerical solution of the integral equations, as well as additional data, can be found in the supplement [21]. We briefly summarize the approximate analytical solutions to the equations in Fig. 1 in the normal state, obtained earlier for a quadratic fermion band [7, 33]: The bosonic self-energy $\Pi(i\omega) \sim g'^2 \mathcal{N}^2 |\omega|$, where \mathcal{N} is the fermionic density of states, leading to an overdamped bosonic dynamics with dynamic exponent $z = 2$; the fermion self-energy has a marginal Fermi-liquid [47] form $\Sigma(i\omega) \sim ig'^2 \mathcal{N} \omega \log(|\omega|)$. The marginal Fermi liquid behavior does not extend to transport properties with a spatially uniform Yukawa coupling g [7], but does with the spatially random g' : the resistivity was found to be T -linear up to logarithmic corrections, $\rho \sim g'^2 T \times (\text{logarithmic factors})$.

Our numerical findings for the phase diagram are summarized in Fig. 2a, which is plotted as a function of the renormalized boson mass M used to tune the system to the quantum critical point (QCP), and T . The phenomenology is broadly similar to that observed experimentally in a wide variety of strange metals: Above the QCP there is a quantum-critical fan, in which the resistivity has an approximately linear T dependence. At low T the QCP is ultimately masked by a superconducting phase, with the maximal T_c occurring at the critical point. The d.c. transport is shown in more detail in Fig. 2b. Evidently, the logarithmic corrections to the resistivity mentioned above are relatively weak for the parameters we have considered. On the disordered side of the transition the resistivity is T -linear at elevated T inside the quantum critical fan, before going to zero with

what is well-approximated by a T^2 power-law below a certain crossover temperature. Over the entire T range shown the resistivity is smaller than the quantum of resistance; the system is not a bad metal.

We now consider the finite-frequency response [48]. The real and imaginary parts of the optical conductivity are presented in Figs. 3a and b. At a crude level, the optical conductivity can be seen to have an approximately Drude-like behavior. To better understand the more detailed structure encoded in $\sigma(\omega)$ we follow Michon *et. al.* [6] and parametrize $\sigma(\omega)$ via a 'generalized' Drude formula:

$$\sigma(\omega) = i \frac{e^2 K / 2}{\omega m^*(\omega) / m + i / \tau_{\text{tr}}(\omega)}. \quad (3)$$

Here K is the optical weight and is equal to the average electronic kinetic energy (see (S31) in the supplement [21]). With K defined in this way, we may read off a frequency-dependent transport scattering rate $1/\tau_{\text{tr}}(\omega)$ and frequency dependent mass-enhancement parameter $m^*(\omega)/m$ directly from the real and imaginary parts of the optical conductivity, respectively.

The optical scattering rate is shown in Fig. 3c. There is an approximately linear in frequency dependence down to $\omega \sim T$, while for frequencies $\omega \lesssim T$ the $1/\tau_{\text{tr}}$ tends to a T -dependent non-zero value which vanishes in the limit $T \rightarrow 0$. The larger ω values of the dimensionless ratio $1/[\omega \tau_{\text{tr}}(\omega)]$ in Fig. 3c is smaller than the observed value [6], but larger values of the ratio appear at larger g' , as shown in Fig. S9b [21].

The frequency-dependent mass enhancement parameter is shown in Fig. 3d. For the chosen parameters, the low-frequency mass enhancement does not exceed roughly 20% down to the lowest temperatures we are able to reliably access in the numerical calculations. The behavior of this "optical" mass enhancement is consistent with the mass enhancement we have inferred from the fermion self-energy [21]. At sufficiently low temperatures $m^*(\omega = 0)/m$ is expected to diverge logarithmically with T [7]. While we do not observe a pure logarithmic growth of m^*/m in our data, the mass enhancement does continuously increase with decreasing T at the QCP, suggesting a (slow) divergence as $T \rightarrow 0$.

We also report the modulus and phase of the optical conductivity in Figs. 3e and f. Notably, we find the modulus of the conductivity has an apparent sub-linear power law behavior over an intermediate frequency range $|\sigma| \sim 1/\omega^{\nu^*}$, where $\nu^* \simeq 0.9$ for the chosen set of parameters. Over a similar frequency range the phase of the optical conductivity plateaus at a value $\arg \sigma \simeq \nu^* \pi / 2$. Such behavior at intermediate frequencies has been observed in infrared conductivity measurements of cuprates [5, 6, 49]. The exponent ν^* is continuously tunable with parameters and, in particular, is a decreasing function of the coupling strength g' [21].

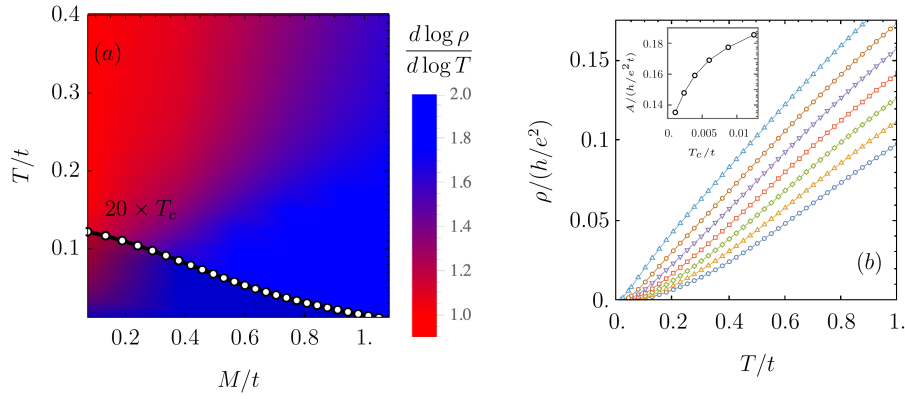


FIG. 2: (a) Normal state resistivity exponent as a function of T and M , the $T = 0$ value of the renormalized boson mass, which tunes away from the quantum critical point at $M = 0$ [21], together with the superconducting T_c . Here the relatively small T_c values have been multiplied to be put on the same scale as resistivity data. (b) Normal state resistivity for different values of M . From bottom to top: $M/t = 1.3, 1.1, 0.9, 0.7, 0.6, 0.4, 0$. The inset plots A , the co-efficient of the linear- T resistivity, versus the superconducting T_c .

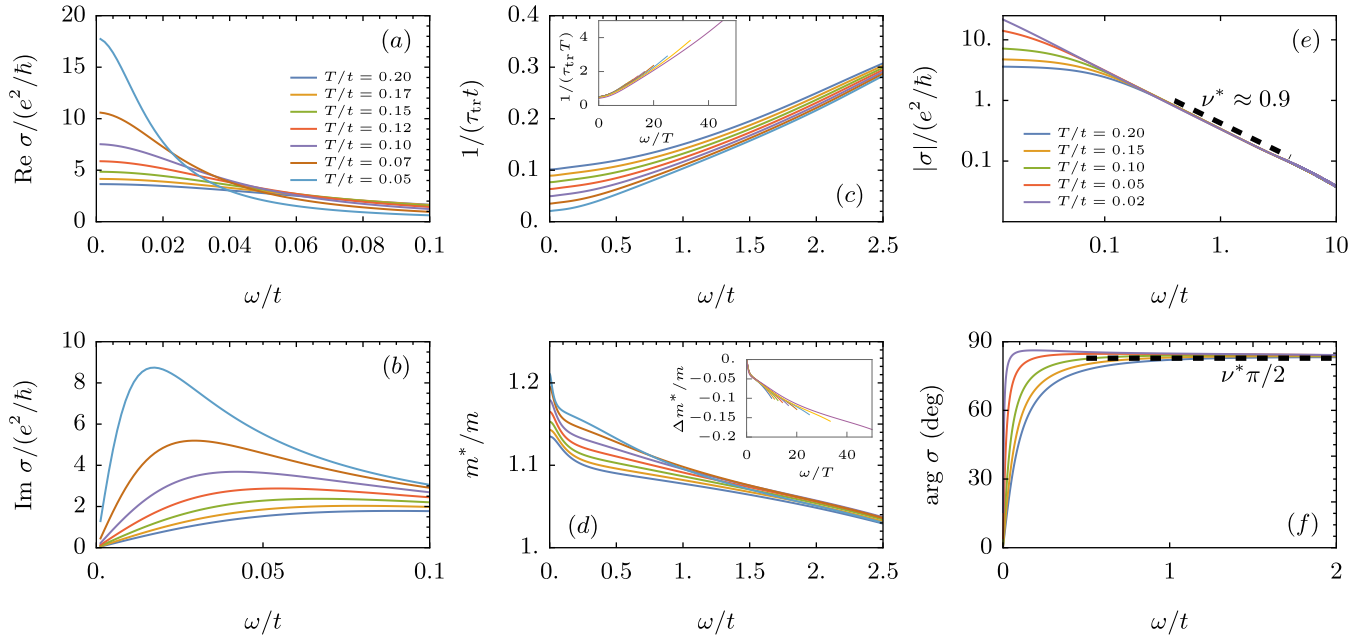


FIG. 3: (a,b) Normal state optical conductivity at the quantum critical coupling for various temperatures indicated in Panel (a). (c,d) Transport scattering rate $1/\tau_{tr}$ and effective mass m^* obtained from σ using (3); inset of Panel (c) is a scaling plot with $1/\tau_{tr}$ and ω scaled by T , inset of Panel (d) is a scaling plotting showing $\Delta m^*/m = m^*(\omega)/m - m^*(0)/m$ as a function of ω/T . (e,f) Modulus and phase of $\sigma(\omega)$. The effective exponent ν^* is explained in the text. Temperatures ranges are the same for Panels (a)-(d) and for Panels (e) and (f). Our results match the trends of the observations in Figs 3a,3b,1c,2b,1d,2d of Ref. 6.

Within the quantum critical fan, frequency-dependent observables are generally expected to obey ω/T scaling. In the present model, ω/T scaling for the optical conductivity is spoiled by logarithmic corrections [6, 7], the most significant such effect arising from the logarithmic divergence of the effective mass with T . This may be accounted for by utilizing the generalized Drude formula

(3) and considering separately ω/T scaling of $1/\tau_{tr}$ and $\Delta m^*/m = m^*(\omega)/m - m^*(0)/m$, where the subtraction removes a contribution that is expected to violate scaling. With this approach we find reasonable scaling collapse for the optical scattering rate – see inset of Fig. 3c. For the parameters presented here, significant logarithmic corrections apparently remain for $\Delta m^*/m$. To the

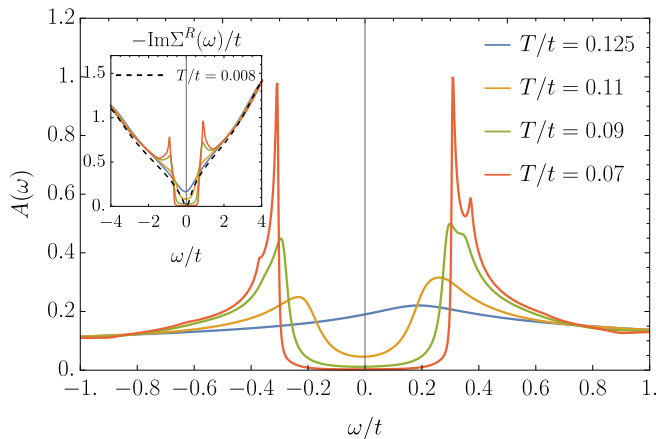


FIG. 4: Evolution of the local density of states upon cooling through T_c at the QCP for strong coupling $g'/t^{3/2} = 5$. Inset shows the marginal Fermi-liquid form of the fermion self-energy $-\text{Im}\Sigma \sim |\omega|$ at the QCP. Dashed curve is calculated in the normal state at $T/t = 0.008$.

extent there is any reasonable scaling collapse, it only holds over a much narrow range of ω/T – see inset of Fig. 3d.

Superconductivity Results—We now investigate the onset of superconducting pairing in our theory. The superconducting transition temperature T_c , as shown in Fig. 2a, is numerically identified by the linearized gap equation; see Appendix SIII. For fixed g' , as we tune away from the QCP by increasing the renormalized boson mass M , we find that T_c decreases. We compare T_c with A , the slope of the linear- T resistivity, in the inset of Fig. 2b. The relation is monotonic, but not linear as discussed by Taillefer [18]. We note, however, that in [18] the coefficient A was not extracted in the quantum-critical fan, which is how we have defined it, but rather from fitting to the low- T resistivity in an “extended” critical regime – this regime has been associated with the localization of ϕ [8], and is not addressed by our analysis here. If we remain at criticality while changing g' , then we do find a linear relationship between A and T_c , as shown in Fig. S5a [21].

In Fig. 4 we show the evolution of the electronic density of states at the quantum critical point as the system goes through the superconducting transition, demonstrating an apparently conventional gap opening as temperatures decreases to $T < T_c$ despite the fact that, in the absence of superconductivity, the fermions behave as a marginal Fermi liquid with $-\text{Im}\Sigma \sim |\omega|$ at low T , as seen in the inset of Fig. 4.

We have also computed the superfluid stiffness, which may be expressed in terms of the anomalous Matsubara

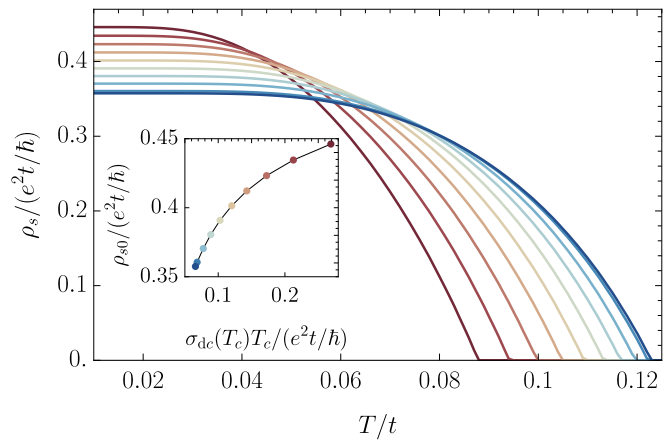


FIG. 5: Temperature dependence of superfluid stiffness ρ_s at $g'/t^{3/2} = 5$ and $v = 0$ for various values of renormalized boson mass M . Inset: The plot of zero temperature superfluid density ρ_{s0} vs $\sigma_{\text{dc}}(T_c)T_c$. From dark red to dark blue (critical point): $M/t = 1.7, 1.5, 1.4, 1.2, 1, 0.8, 0.7, 0.4, 0.1, 0$.

Green’s function F as

$$\frac{\rho_s}{\pi e^2} = \frac{2}{\beta} \sum_{\omega_n} \int d\epsilon \rho_{\text{tr}}(\epsilon) F(\epsilon, i\omega_n) F^\dagger(\epsilon, i\omega_n), \quad (4)$$

where the density of states $\rho_{\text{tr}}^{\alpha\beta}(\epsilon) \equiv \int_{\mathbf{k}} \frac{\partial \epsilon_{\mathbf{k}}}{\partial k_\alpha} \frac{\partial \epsilon_{\mathbf{k}}}{\partial k_\beta} \delta(\epsilon - \epsilon_{\mathbf{k}})$. In Fig. 5, we show the temperature dependence of ρ_s for $g' = 5t^{3/2}$ as the system is tuned away from the QCP by varying the boson mass M . The stiffness reaches a finite constant value, ρ_{s0} , for $T \rightarrow 0$. As the system is tuned away from the QCP, T_c decreases from its maximal value while ρ_{s0} increases, as seen in Fig. 5. This result at strong coupling aligns with the superfluid density in bulk samples of the overdoped cuprate superconductors [19, 50]. When T_c is largest at the QCP, the opening of a ψ gap at $T = 0$ weakens the pairing interaction mediated by ϕ (because the ϕ self energy Π is self-consistently determined by the ψ polarization, see Fig. 1), leading to a smaller superfluid stiffness at $T = 0$ [16, 17]. On the other hand, in the presence of strong potential scattering v this effect is weaker, and a decreasing T_c is eventually accompanied by a decreasing ρ_{s0} , as shown in Fig. S12 [21].

Homes’ Law [20] postulates a universal value for the dimensionless ratio $\rho_{s0}/(T_c \sigma_{\text{dc}}(T_c))$, where $\sigma_{\text{dc}}(T_c)$ is the normal state d.c. conductivity at T_c : we investigate this relationship in the inset of Fig. 5 and Section SV [21]. In the presence of a non-zero v , we find in Section SV a linear relation between ρ_{s0} and $T_c \sigma_{\text{dc}}(T_c)$, with a slope which can be close to the experimentally observed value.

Discussion—The spatially inhomogeneous fermion-boson coupling $g'(\mathbf{r})$ in the 2d-YSYK model in (1) is an alternative to ‘random mass’ $\delta s(\mathbf{r})$ disorder in Hertz-Millis theory, in the crossover regime where the bosonic

modes remain extended despite the disorder [8], as we discussed below (2). The striking similarities between the results presented here and a variety of properties measured in strange metal superconductors such as the cuprates – including static and dynamic properties across the normal and superconducting states – indicate such disorder plays a significant role in the phenomenology of these systems, making it important to determine the microscopic origin of disorder configurations that strongly affect the local position of the QCP. Finally, the crucial issue of how our results evolve as the bosonic modes localize due to disorder [8] will be addressed in future work.

Acknowledgements—We thank Erez Berg, Christophe Berthod, Andrey Chubukov, Carlo Di Castro, Antoine Georges, Peter Lunts, Dmitrii Maslov, Srinivas Raghu, and Dirk van der Marel for valuable discussions. This research was supported by the U.S. National Science Foundation grant No. DMR-2245246 and by the Simons Collaboration on Ultra-Quantum Matter which is a grant from the Simons Foundation (651440, S.S.). The Flatiron Institute is a division of the Simons Foundation. J.S. and D. V. were supported by the German Research Foundation (DFG) through CRC TRR 288 “ElastoQMat,” project A07. I.E. was supported by the University of Wisconsin–Madison.

-
- [1] S. A. Hartnoll and A. P. Mackenzie, *Colloquium: Planckian dissipation in metals*, *Rev. Mod. Phys.* **94**, 041002 (2022), arXiv:2107.07802 [cond-mat.str-el].
- [2] D. Chowdhury, A. Georges, O. Parcollet, and S. Sachdev, *Sachdev-Ye-Kitaev Models and Beyond: A Window into Non-Fermi Liquids*, arXiv e-prints, arXiv:2109.05037 (2021), arXiv:2109.05037 [cond-mat.str-el].
- [3] S. Ahn and S. Das Sarma, *Planckian properties of two-dimensional semiconductor systems*, *Phys. Rev. B* **106**, 155427 (2022), arXiv:2204.02982 [cond-mat.mes-hall].
- [4] S. Das Sarma and Y.-T. Tu, *Role of many-phonon modes on the high-temperature linear-in- T electronic resistivity*, *Phys. Rev. B* **109**, 235118 (2024), arXiv:2403.09890 [cond-mat.mes-hall].
- [5] D. v. d. Marel, H. J. A. Molegraaf, J. Zaanen, Z. Nussinov, F. Carbone, A. Damascelli, H. Eisaki, M. Greven, P. H. Kes, and M. Li, *Quantum critical behaviour in a high- T_c superconductor*, *Nature (London)* **425**, 271 (2003), arXiv:cond-mat/0309172 [cond-mat.str-el].
- [6] B. Michon, C. Berthod, C. W. Rischau, A. Ataei, L. Chen, S. Komiya, S. Ono, L. Taillefer, D. van der Marel, and A. Georges, *Reconciling scaling of the optical conductivity of cuprate superconductors with Planckian resistivity and specific heat*, *Nature Communications* **14**, 3033 (2023), arXiv:2205.04030 [cond-mat.str-el].
- [7] A. A. Patel, H. Guo, I. Esterlis, and S. Sachdev, *Universal theory of strange metals from spatially random interactions*, *Science* **381**, abq6011 (2023), arXiv:2203.04990 [cond-mat.str-el].
- [8] A. A. Patel, P. Lunts, and S. Sachdev, *Localization of overdamped bosonic modes and transport in strange metals*, *Proc. Nat. Acad. Sci.* **121**, e2402052121 (2024), arXiv:2312.06751 [cond-mat.str-el].
- [9] A. A. Patel, P. Lunts, and M. Albergo, *to appear*, (2024).
- [10] A. B. Harris, *Effect of random defects on the critical behaviour of Ising models*, *Journal of Physics C: Solid State Physics* **7**, 1671 (1974).
- [11] J. T. Chayes, L. Chayes, D. S. Fisher, and T. Spencer, *Finite-Size Scaling and Correlation Lengths for Disordered Systems*, *Phys. Rev. Lett.* **57**, 2999 (1986).
- [12] J. A. Hoyos, C. Kotabage, and T. Vojta, *Effects of Dissipation on a Quantum Critical Point with Disorder*, *Phys. Rev. Lett.* **99**, 230601 (2007), arXiv:0705.1865 [cond-mat.str-el].
- [13] Y. Wang, *Solvable Strong-coupling Quantum Dot Model with a Non-Fermi-liquid Pairing Transition*, *Phys. Rev. Lett.* **124**, 017002 (2020), arXiv:1904.07240 [cond-mat.str-el].
- [14] I. Esterlis and J. Schmalian, *Cooper pairing of incoherent electrons: an electron-phonon version of the Sachdev-Ye-Kitaev model*, *Phys. Rev. B* **100**, 115132 (2019), arXiv:1906.04747 [cond-mat.str-el].
- [15] W. Wang, A. Davis, G. Pan, Y. Wang, and Z. Y. Meng, *Phase diagram of the spin-1/2 Yukawa-Sachdev-Ye-Kitaev model: Non-Fermi liquid, insulator, and superconductor*, *Phys. Rev. B* **103**, 195108 (2021), arXiv:2102.10755 [cond-mat.str-el].
- [16] D. Valentinis, G. A. Inkof, and J. Schmalian, *BCS to incoherent superconductivity crossovers in the Yukawa-SYK model on a lattice*, *Phys. Rev. B* **108**, L140501 (2023), arXiv:2302.13138 [cond-mat.supr-con].
- [17] D. Valentinis, G. A. Inkof, and J. Schmalian, *Correlation between phase stiffness and condensation energy across the non-Fermi to Fermi-liquid crossover in the Yukawa-Sachdev-Ye-Kitaev model on a lattice*, *Phys. Rev. Res.* **5**, 043007 (2023), arXiv:2302.13134 [cond-mat.supr-con].
- [18] L. Taillefer, *Scattering and Pairing in Cuprate Superconductors*, *Annual Review of Condensed Matter Physics* **1**, 51 (2010), arXiv:1003.2972 [cond-mat.supr-con].
- [19] S. V. Dordevic and C. C. Homes, *Superfluid density in overdoped cuprates: Thin films versus bulk samples*, *Phys. Rev. B* **105**, 214514 (2022), arXiv:2206.13987 [cond-mat.supr-con].
- [20] C. C. Homes, S. V. Dordevic, M. Strongin, D. A. Bonn, R. Liang, W. N. Hardy, S. Komiya, Y. Ando, G. Yu, N. Kaneko, X. Zhao, M. Greven, D. N. Basov, and T. Timusk, *A universal scaling relation in high-temperature superconductors*, *Nature (London)* **430**, 539 (2004), arXiv:cond-mat/0404216 [cond-mat.supr-con].
- [21] *Supplementary material attached.*, .
- [22] S. A. Hartnoll, P. K. Kovtun, M. Muller, and S. Sachdev, *Theory of the Nernst effect near quantum phase transitions in condensed matter, and in dyonic black holes*, *Phys. Rev. B* **76**, 144502 (2007), arXiv:0706.3215 [cond-mat.str-el].
- [23] D. L. Maslov, V. I. Yudson, and A. V. Chubukov, *Resistivity of a Non-Galilean-Invariant Fermi Liquid near Pomeranchuk Quantum Criticality*, *Phys. Rev. Lett.* **106**, 106403 (2011), arXiv:1012.0069 [cond-mat.str-el].
- [24] S. A. Hartnoll, R. Mahajan, M. Punk, and S. Sachdev, *Transport near the Ising-nematic quantum critical point of metals in two dimensions*, *Phys. Rev. B* **89**, 155130 (2014), arXiv:1401.7012 [cond-mat.str-el].
- [25] A. A. Patel and S. Sachdev, *dc resistivity at the onset of spin density wave order in two-dimensional metals*,

- Phys. Rev. B **90**, 165146 (2014), arXiv:1408.6549 [cond-mat.str-el].
- [26] D. L. Maslov and A. V. Chubukov, *Optical response of correlated electron systems*, *Reports on Progress in Physics* **80**, 026503 (2017), arXiv:1608.02514 [cond-mat.str-el].
- [27] H. Guo, A. A. Patel, I. Esterlis, and S. Sachdev, *Large- N theory of critical Fermi surfaces. II. Conductivity*, *Phys. Rev. B* **106**, 115151 (2022), arXiv:2207.08841 [cond-mat.str-el].
- [28] Z. D. Shi, D. V. Else, H. Goldman, and T. Senthil, *Loop current fluctuations and quantum critical transport*, *SciPost Phys.* **14**, 113 (2023), arXiv:2208.04328 [cond-mat.str-el].
- [29] H. Guo, D. Valentinis, J. Schmalian, S. Sachdev, and A. A. Patel, *Cyclotron resonance and quantum oscillations of critical Fermi surfaces*, *Phys. Rev. B* **109**, 075162 (2024), arXiv:2308.01956 [cond-mat.supr-con].
- [30] H. V. Löhneysen, A. Rosch, M. Vojta, and P. Wölfle, *Fermi-liquid instabilities at magnetic quantum phase transitions*, *Rev. Mod. Phys.* **79**, 1015 (2007), arXiv:cond-mat/0606317 [cond-mat.str-el].
- [31] S. Sachdev, *Strange metals and black holes: insights from the Sachdev-Ye-Kitaev model*, Oxford Research Encyclopedia in Physics 10.1093/acrefore/9780190871994.013.48 (2023), arXiv:2305.01001 [cond-mat.str-el].
- [32] E. E. Aldape, T. Cookmeyer, A. A. Patel, and E. Altman, *Solvable theory of a strange metal at the breakdown of a heavy Fermi liquid*, *Phys. Rev. B* **105**, 235111 (2022), arXiv:2012.00763 [cond-mat.str-el].
- [33] I. Esterlis, H. Guo, A. A. Patel, and S. Sachdev, *Large N theory of critical Fermi surfaces*, *Phys. Rev. B* **103**, 235129 (2021), arXiv:2103.08615 [cond-mat.str-el].
- [34] X.-H. Ge, S.-J. Sin, and Y.-L. Wang, *Linear- T Resistivity from Spatially Random Vector Coupling*, (2024), arXiv:2406.11170 [hep-th].
- [35] P. A. Lee and T. V. Ramakrishnan, *Disordered electronic systems*, *Rev. Mod. Phys.* **57**, 287 (1985).
- [36] W. Fu, D. Gaiotto, J. Maldacena, and S. Sachdev, *Supersymmetric Sachdev-Ye-Kitaev models*, *Phys. Rev. D* **95**, 026009 (2017), [Addendum: Phys.Rev.D 95, 069904 (2017)], arXiv:1610.08917 [hep-th].
- [37] J. Murugan, D. Stanford, and E. Witten, *More on Supersymmetric and 2d Analogs of the SYK Model*, *JHEP* **08**, 146, arXiv:1706.05362 [hep-th].
- [38] A. A. Patel and S. Sachdev, *Critical strange metal from fluctuating gauge fields in a solvable random model*, *Phys. Rev. B* **98**, 125134 (2018), arXiv:1807.04754 [cond-mat.str-el].
- [39] E. Marcus and S. Vandoren, *A new class of SYK-like models with maximal chaos*, *JHEP* **01**, 166, arXiv:1808.01190 [hep-th].
- [40] Y. Wang and A. V. Chubukov, *Quantum Phase Transition in the Yukawa-SYK Model*, *Phys. Rev. Res.* **2**, 033084 (2020), arXiv:2005.07205 [cond-mat.str-el].
- [41] H. Hosseinabadi, S. P. Kelly, J. Schmalian, and J. Marino, *Thermalization of non-Fermi-liquid electron-phonon systems: Hydrodynamic relaxation of the Yukawa-Sachdev-Ye-Kitaev model*, *Phys. Rev. B* **108**, 104319 (2023), arXiv:2306.03898 [cond-mat.str-el].
- [42] M. Milovanović, S. Sachdev, and R. N. Bhatt, *Effective-field theory of local-moment formation in disordered metals*, *Phys. Rev. Lett.* **63**, 82 (1989).
- [43] N. Bashan, E. Tulipman, J. Schmalian, and E. Berg, *Tunable Non-Fermi Liquid Phase from Coupling to Two-Level Systems*, *Phys. Rev. Lett.* **132**, 236501 (2024), arXiv:2310.07768 [cond-mat.str-el].
- [44] E. Tulipman, N. Bashan, J. Schmalian, and E. Berg, *Solvable models of two-level systems coupled to itinerant electrons: Robust non-Fermi liquid and quantum critical pairing*, (2024), arXiv:2404.06532 [cond-mat.str-el].
- [45] T. C. Wu, Y. Liao, and M. S. Foster, *Quantum interference of hydrodynamic modes in a dirty marginal Fermi liquid*, *Phys. Rev. B* **106**, 155108 (2022), arXiv:2206.01762 [cond-mat.str-el].
- [46] M. Grilli, C. Di Castro, G. Mirarchi, G. Seibold, and S. Caprara, *Dissipative quantum criticality as a source of strange metal behavior*, *Symmetry* **15**, 569 (2023), arXiv:2205.10876 [cond-mat.str-el].
- [47] C. M. Varma, P. B. Littlewood, S. Schmitt-Rink, E. Abrahams, and A. E. Ruckenstein, *Phenomenology of the normal state of Cu-O high-temperature superconductors*, *Phys. Rev. Lett.* **63**, 1996 (1989).
- [48] The related problem of optical conductivity at a clean Ising-nematic QCP has been recently analyzed in [51, 52].
- [49] M. R. Norman and A. V. Chubukov, *High-frequency behavior of the infrared conductivity of cuprates*, *Phys. Rev. B* **73**, 140501 (2006).
- [50] J. Hwang, T. Timusk, and G. D. Gu, *Doping dependent optical properties of $Bi_2Sr_2CaCu_2O_{8+\delta}$* , *Journal of Physics Condensed Matter* **19**, 125208 (2007), arXiv:cond-mat/0607653 [cond-mat.supr-con].
- [51] S. Li, P. Sharma, A. Levchenko, and D. L. Maslov, *Optical conductivity of a metal near an Ising-nematic quantum critical point*, *Phys. Rev. B* **108**, 235125 (2023), arXiv:2309.12571 [cond-mat.str-el].
- [52] Y. Gindikin and A. V. Chubukov, *Fermi surface geometry and optical conductivity of a two-dimensional electron gas near an Ising-nematic quantum critical point*, *Phys. Rev. B* **109**, 115156 (2024), arXiv:2401.17392 [cond-mat.str-el].

SUPPLEMENT TO

Strange metal and superconductor in the two-dimensional Yukawa-SYK model

Chenyuan Li,¹ Davide Valentini,^{2,3} Aavishkar A. Patel,⁴
Haoyu Guo,⁵ Jörg Schmalian,^{2,3} Subir Sachdev,¹ and Ilya Esterlis⁶

¹*Department of Physics, Harvard University, Cambridge MA 02138, USA*

²*Institut für Quantenmaterialien und Technologien,
Karlsruher Institut für Technologie, 76131 Karlsruhe, Germany*

³*Institut für Theorie der Kondensierten Materie,
Karlsruher Institut für Technologie, 76131 Karlsruhe, Germany*

⁴*Center for Computational Quantum Physics,
Flatiron Institute, New York, New York, 10010, USA*

⁵*Laboratory of Atomic and Solid State Physics, Cornell University,
142 Sciences Drive, Ithaca NY 14853-2501, USA*

⁶*Department of Physics, University of Wisconsin-Madison, Madison, Wisconsin 53706, USA*

(Dated: June 19, 2024)

The plan of the supplement is as follows. We introduce our model, its averaged effective action, and the setup of the large- N expansion in Section [SI](#). This involves a path integral over a $G - \Sigma$ action in which the fields are bilocal in spacetime. A full numerical solution of the large N equations for the complete Fermi surface is obtained in Section [SII](#) for complex couplings and [SIII](#) for real couplings. We present the normal state and superconducting solutions and find results which are in agreement with the previous analysis. We then discuss transport properties in Section [SIV](#), and Homes' Law in Section [SV](#).

SI. THE 2d-YSYK MODEL AND ITS SADDLE-POINT EQUATIONS

We endow the fermions and bosons with an additional flavor index i, j, ℓ , and the fermions with a spin index σ , and work the following lattice action in imaginary time

$$\begin{aligned}
S = & \int d\tau d^2x \sum_{i=1}^N \sum_{\sigma=\pm 1} \psi_{i\sigma}^\dagger(\tau, x) [\partial_\tau + \epsilon_k] \psi_{i\sigma}(\tau, x) + \frac{1}{2} \int d\tau d^2x \sum_{i=1}^N \phi_i(\tau, x) [-\partial_\tau^2 + \omega_q^2] \phi_i(\tau, x) \\
& + \int d^2\tau dx \sum_{i,j}^N \sum_{\sigma=\pm 1} \frac{v_{ij}(x)}{\sqrt{N}} \psi_{i\sigma}^\dagger(\tau, x) \psi_{j\sigma}(\tau, x) \\
& + \int d\tau d^2x \sum_{i,j,\ell=1}^N \sum_{\sigma=\pm 1} \frac{g'_{ij\ell}(x)}{N} \psi_{i\sigma}^\dagger(\tau, x) \psi_{j\sigma}(\tau, x) \phi_\ell(\tau, x), \tag{S1}
\end{aligned}$$

with the following choice of lattice dispersion

$$\epsilon_k = -2t(\cos k_x + \cos k_y) - \mu, \tag{S2a}$$

$$\omega_q^2 = m_b^2 + 2J(2 - \cos q_x - \cos q_y). \tag{S2b}$$

Here t is the fermion hopping, μ is the chemical potential, m_b is the bare boson mass and the stiffness J determines the boson dispersion. The Yukawa couplings $g'_{ij\ell}$ are complex-valued random variables that obey $g'_{ij\ell}(x) = g_{1,ij\ell}(x) + ig_{2,ij\ell}(x) = g'_{ji\ell}(x)$. The real part $g_{1,ij\ell}(x)$ and the imaginary part $g_{2,ij\ell}(x)$ have zero mean and the variances are [\[1\]](#)

$$\begin{aligned}
\overline{g_{1,ij\ell}(x)g_{1,i'j'\ell'}(x')} &= \left(1 - \frac{\alpha}{2}\right) g'^2 \delta_{\ell,\ell'} (\delta_{ii'}\delta_{jj'} + \delta_{ij'}\delta_{ji'}) \delta(x - x'), \\
\overline{g_{2,ij\ell}(x)g_{2,i'j'\ell'}(x')} &= \frac{\alpha}{2} g'^2 \delta_{\ell,\ell'} (\delta_{ii'}\delta_{jj'} - \delta_{ij'}\delta_{ji'}) \delta(x - x'), \\
\overline{g_{1,ij\ell}(x')g_{2,i'j'\ell'}(x')} &= 0. \tag{S3}
\end{aligned}$$

In the $\alpha = 1$ limit, [\(S3\)](#) reduces to $\langle g'_{ij\ell}(x)g'_{i'j'\ell'}(x')^* \rangle = g'^2 \delta(x - x') \delta_{ii'} \delta_{jj'} \delta_{\ell\ell'}$ and no superconductivity occurs [\[1\]](#). For $\alpha = 0$, however, the coupling constants are all real valued, which

preserves time-reversal symmetry for each realization of the random couplings and thus gives rise to superconductivity. The spatially random potential satisfies

$$\overline{v_{ij}(x)} = 0, \quad \overline{v_{ij}^*(x)v_{i'j'}(x')} = v^2 \delta(x - x')\delta_{ii'}\delta_{jj'}, \quad (\text{S4})$$

After a disorder average via the replica trick, we obtain

$$\begin{aligned} \frac{S}{N} = & -\text{Tr} \log(\hat{G}_0^{-1} - \hat{\Sigma}) + \frac{1}{2} \text{Tr} \log(D_0^{-1} - \Pi) \\ & - \int d\tau d^2x \int d\tau' d^2x' \left(2\Sigma(\tau', x'; \tau, x)G(\tau, x; \tau', x') - \frac{1}{2}\Pi(\tau', x'; \tau, x)D(\tau, x; \tau', x') \right) \\ & - \int d\tau d^2x \int d\tau' d^2x' \left(\Phi^\dagger(\tau', x'; \tau, x)F(\tau, x; \tau', x') + \Phi(\tau', x'; \tau, x)F^\dagger(\tau, x; \tau', x') \right) \\ & + v^2 \int d\tau d^2x \int d\tau' d^2x' \left(G(\tau, x; \tau', x')G(\tau', x'; \tau, x) - (1 - \alpha)F^\dagger(\tau, x; \tau', x')F(\tau', x'; \tau, x) \right) \delta(x - x') \\ & + g^2 \int d\tau d^2x \int d\tau' d^2x' G(\tau, x; \tau', x')G(\tau', x'; \tau, x)D(\tau, x; \tau', x') \delta(x - x') \\ & - g^2(1 - \alpha) \int d\tau d^2x \int d\tau' d^2x' F^\dagger(\tau, x; \tau', x')F(\tau', x'; \tau, x)D(\tau, x; \tau', x') \delta(x - x') \\ & - \int d\tau d^2x \frac{i\lambda(\tau, x)}{2} \left(\sum_{i=1}^N \phi_i(\tau, x)\phi_i(\tau, x) - N/\gamma \right). \end{aligned} \quad (\text{S5})$$

Here \hat{G}_0^{-1} and $\hat{\Sigma}$ are matrices in Nambu space. We have introduced the time-bilocal fields G , F , D , which are normal and anomalous fermionic Green's functions, as well as bosonic Green's functions. The corresponding self-energies, given by Σ , Φ and Π , are employed as Lagrange multipliers. To tune the system to criticality, we have found it most convenient to first impose a fixed length constraint [2]:

$$\sum_q \sum_{i=1}^N \phi_{iq}(\tau)\phi_{i,-q}(\tau) = N/\gamma, \quad (\text{S6})$$

which is implemented by the Lagrange multiplier λ Eq.(S6) and implicitly determines m_b^2 , and use γ as tuning parameter to access the QCP. In the main text we present the phase diagram in terms of the $T = 0$ value of the renormalized boson mass $M^2 = m_b^2 - \Pi(\omega = 0, T = 0)$.

Integrating out ψ and ϕ yields this G - Σ action (S5). In the limit of a large number of flavors,

the SYK-type saddle-point equations are given by

$$\hat{G}(i\omega) = \int \frac{d^2k}{(2\pi)^2} \left(i\omega\sigma_0 + \mu\sigma_3 - \varepsilon_k\sigma_3 - \hat{\Sigma}(i\omega) \right)^{-1}, \quad (\text{S7a})$$

$$D(i\nu) = \int \frac{d^2q}{(2\pi)^2} \frac{1}{\nu^2 + \omega_q^2 + m_b^2 - \Pi(i\nu)}, \quad (\text{S7b})$$

$$\Sigma(\tau) = g'^2 G(\tau) D(\tau) + v^2 G(\tau), \quad (\text{S7c})$$

$$\Phi(\tau) = -(1 - \alpha)(g'^2 F(\tau) D(\tau) + v^2 F(\tau)), \quad (\text{S7d})$$

$$\Pi(\tau) = -2g'^2 (G(\tau)G(-\tau) - (1 - \alpha)F(\tau)F^\dagger(-\tau)), \quad (\text{S7e})$$

$$\frac{1}{\gamma} = T \sum_\nu \int \frac{d^2q}{(2\pi)^2} \frac{1}{\nu^2 + \omega_q^2 + m_b^2 - \Pi(i\nu)}. \quad (\text{S7f})$$

These equations are indicated schematically in Figure 1 for $v = 0$. Different from the translationally invariant model, the self-energies are momentum independent as a result of the extra δ -function in (S5). In section SII and SIII we will present numerical solutions of these equations.

SII. NUMERICAL SOLUTIONS TO THE COMPLEX 2d-YSYK MODEL

We first solve the saddle-point equations in the normal state and consider complex-valued $g'_{ij\ell}$ extracted from the Gaussian unitary ensemble ($\alpha = 1$)[1, 3]. In this limit, the anomalous terms disappear and saddle point equations (S7a)-(S7e) are simplified as

$$\Sigma(i\omega_n) = g'^2 T \sum_m G(i\omega_n - i\nu_m) D(i\nu_m) + v^2 G(i\omega_n), \quad (\text{S8a})$$

$$\Pi(i\nu_n) = -2g'^2 T \sum_m G(i\nu_n + i\omega_m) G(i\omega_m), \quad (\text{S8b})$$

$$G(i\omega_n) = \int \frac{d^2k}{(2\pi)^2} \frac{1}{i\omega_n - \varepsilon_k + \mu - \Sigma(i\omega_n)}, \quad (\text{S8c})$$

$$D(i\nu_n) = \int \frac{d^2q}{(2\pi)^2} \frac{1}{\nu_n^2 + \omega_q^2 + m_b^2 - \Pi(i\nu_n)}. \quad (\text{S8d})$$

For the lattice dispersion (S2), the momentum integrations for the local Green's functions can be worked out analytically, giving rise to the local Green's function

$$G_{\text{loc}}(z) = \frac{1}{4t} \mathcal{G} \left(\frac{z + \mu - \Sigma(z)}{4t} \right). \quad (\text{S9})$$

Here we define

$$\mathcal{G}(z) \equiv \frac{2}{\pi z} K(1/z^2), \quad (\text{S10})$$

with K the complete elliptic integral of the first kind. Similarly, for the bosons we obtain

$$D_{\text{loc}}(z) = \frac{1}{4J} \mathcal{G} \left(\frac{z^2 - m_b^2 - 4J - \Pi(z)}{4J} \right), \quad (\text{S11})$$

where m_b^2 is obtained by solving the above equations with the constraint (S7f)

$$D_{\text{loc}}(\tau = 0) = -\frac{1}{\gamma}. \quad (\text{S12})$$

The value of m_b^2 thus obtained will be plugged into the equations expressed on the real-axis below. Notice that because we have taken care of the momentum integration analytically, we work directly in the thermodynamic limit. The integral equations above are most efficiently solved via fast Fourier transform (FFT). In our calculations, we have used the imaginary time-Matsubara frequency FFT approach described in Ref. [4].

The real-axis version of (S8) originates from the analytic continuation $i\omega_n \rightarrow \omega + i0^+$ of imaginary propagators. To proceed, we introduce the following spectral functions

$$A(\omega) = -\frac{1}{\pi} \text{Im}G^R(\omega), \quad (\text{S13a})$$

$$B(\omega) = -\frac{1}{\pi} \text{Im}D^R(\omega), \quad (\text{S13b})$$

where $G^R(\omega) = G(i\omega_n)|_{i\omega_n \rightarrow \omega + i0^+}$ and $D^R(\omega) = D(i\nu_n)|_{i\nu_n \rightarrow \omega + i0^+}$ are the retarded Green's functions. From the spectral representation, we derive the following retarded self energies

$$\Sigma_R(\omega) = g'^2 \int_{\omega'} \left[\tilde{A}(\omega') D_R(\omega - \omega') - \tilde{B}(\omega') G_R(\omega + \omega') \right] + v^2 G_R(\omega), \quad (\text{S14a})$$

$$\Pi_R(\omega) = g'^2 \int_{\omega'} \tilde{A}(\omega') ([G_R(\omega' - \omega)]^* + G_R(\omega + \omega')), \quad (\text{S14b})$$

Here we define $\tilde{A}(\omega) \equiv A(\omega)n_F(\omega)$ and $\tilde{B}(\omega) \equiv B(\omega)n_B(\omega)$. This approach is similar to that developed in [5].

Numerical results in this section are presented for the fermion chemical potential $\mu = -0.5t$, boson stiffness $J = t^2$, and impurity potential $v = 0$.

A. Boson properties

The temperature-dependent renormalized boson mass is $M^2(T) = m_b^2 - \Pi(\omega = 0, T)$ [2]. At the QCP, $M^2(T) \sim T$ at low temperatures (up to logarithms), as is seen in the left panel of Figure S1. When we simply write M^2 , we refer to the $T = 0$ value $M^2 = M^2(T = 0)$. The retarded boson self-energy shown in Figure S1 obeys $-\text{Im}\Pi_R \sim \omega$, the expected Landau damping form, corresponding to dynamical exponent $z = 2$. The low-frequency behavior is essentially independent of the distance to the QCP.

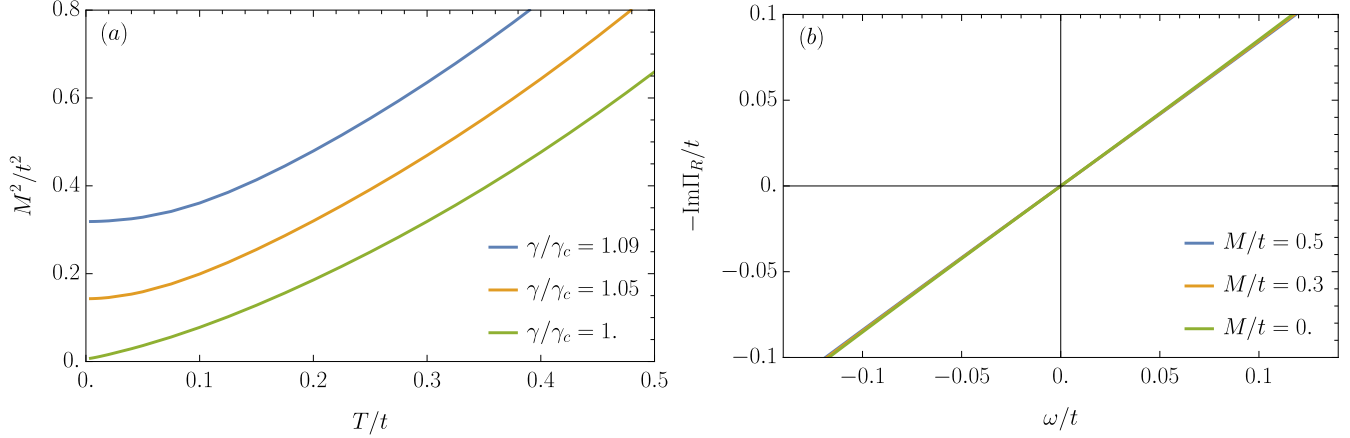


FIG. S1: (a) Renormalized boson mass as a function of T at $g'/t^{3/2} = 2$ for $\gamma \geq \gamma_c$, where γ_c is the QCP and $\gamma > \gamma_c$ corresponds the Fermi-liquid side of the phase diagram. (b) Imaginary part of the bosonic self-energy as a function of ω/t at $T/t = 0.004$ for different values of $T = 0$ boson mass.

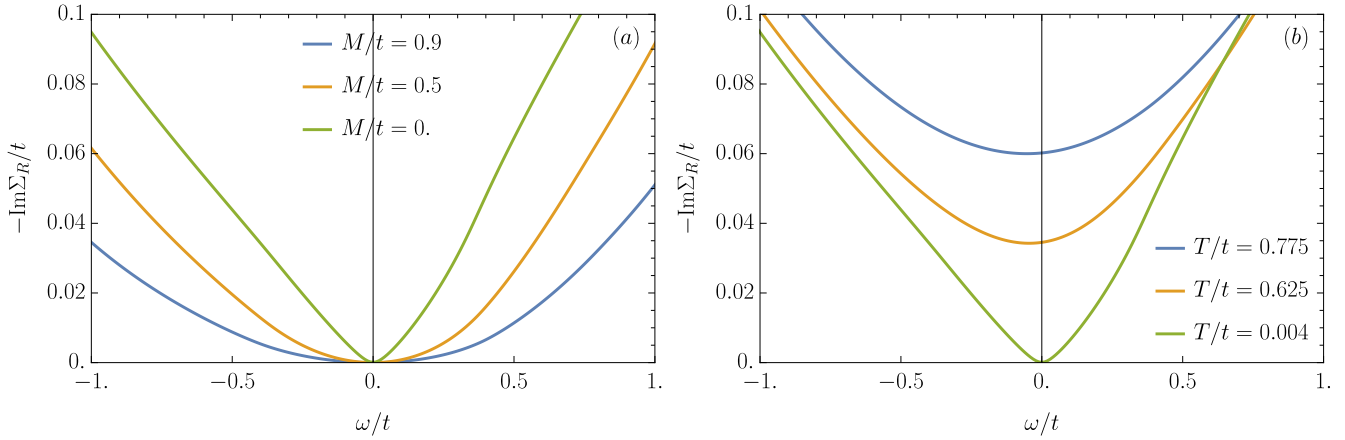


FIG. S2: (a) Imaginary part of the fermionic self-energy as a function of ω/t at $T/t = 0.004$, $g'/t^{3/2} = 2$ for different values of the boson mass. (b) Same as (a) but at the QCP for different temperatures.

B. Fermion properties

Figure S2 shows the imaginary part of the fermionic self-energy, which has the expected forms: a marginal Fermi liquid at the QCP, $-\text{Im}\Sigma_R \sim |\omega|$, and $-\text{Im}\Sigma_R \sim \omega^2$ in the FL regime. The mass enhancement extracted from the fermion self-energy is shown in Fig. S3.

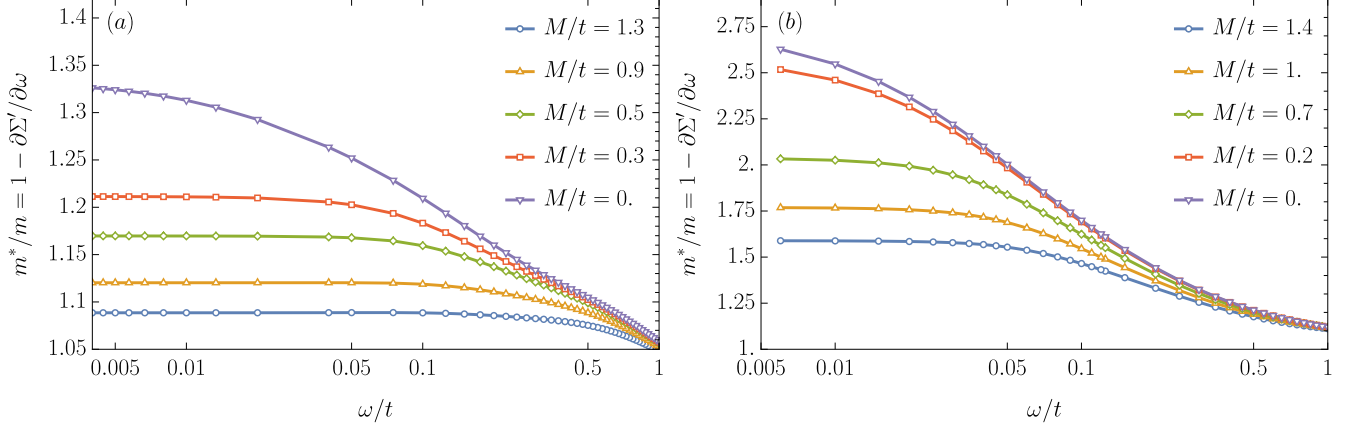


FIG. S3: Enhancement of the effective mass as a function of T/t for different values of boson mass. (a) $g'/t^{3/2} = 2$ (weak coupling) (b) $g'/t^{3/2} = 5$ (strong coupling).

SIII. NUMERICAL SOLUTIONS TO THE REAL 2d-YSYK MODEL

A. Linearized gap equations and T_c

Now we turn to real-valued g'_{ijl} extracted from the Gaussian orthogonal ensemble [1, 3], and start from the linearized gap equations

$$\Phi(i\omega_n) = g'^2(1 - \alpha)T \sum_m D(i\omega_n - i\omega_m)X(i\omega_m)\Phi(i\omega_m) + v^2(1 - \alpha)X(i\omega_n)\Phi(i\omega_n). \quad (\text{S15})$$

Here $X(i\omega_m)$ is determined by normal state solutions

$$X(i\omega_m) = \frac{G^N(i\omega_m) - G^N(-i\omega_m)}{2i\omega_m - \Sigma(i\omega_m) + \Sigma(-i\omega_m)}, \quad G^N(i\omega_m) = \frac{1}{4t} \mathcal{G} \left(\frac{i\omega_m + \mu - \Sigma(i\omega_m)}{4t} \right). \quad (\text{S16})$$

After introducing

$$\tilde{\Phi}(i\omega_n) \equiv \Phi(i\omega_n)[1 - v^2(1 - \alpha)X(i\omega_n)], \quad (\text{S17})$$

Eq. S15 reduces to

$$\tilde{\Phi}(i\omega_n) = g'^2(1 - \alpha)T \sum_m D(i\omega_n - i\omega_m) \frac{1}{1/X(i\omega_m) - v^2(1 - \alpha)} \tilde{\Phi}(i\omega_m). \quad (\text{S18})$$

Therefore, the superconducting transition temperature T_c can be determined by imposing that the matrix

$$K_{nm} = g'^2(1 - \alpha)TD(i\omega_n - i\omega_m) \frac{1}{1/X(i\omega_m) - v^2(1 - \alpha)}, \quad (\text{S19})$$

has eigenvalue 1. In Fig. S4, we present the superconducting T_c as a function of tuning parameter

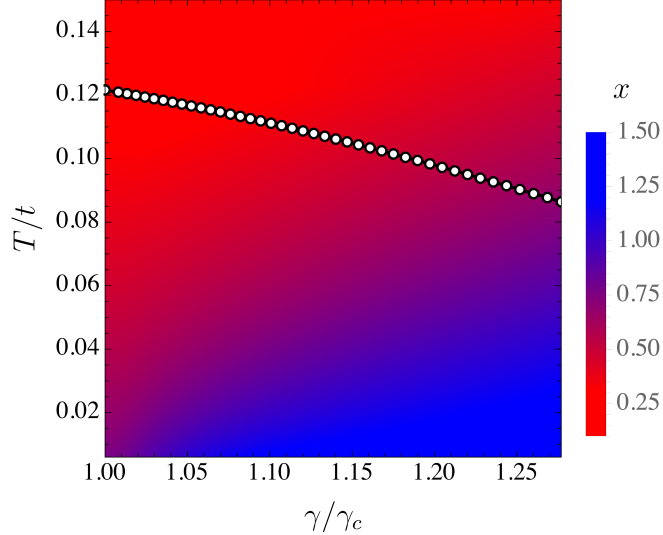


FIG. S4: Phase diagram as $x(\gamma, T/t)$. Up to logarithmic corrections, we expect $x = 1$ (blue) in the quantum critical fan and $x = 2$ in the Fermi liquid regime. White dots indicate T_c . The choice of parameters: $\mu = -0.5t$, $J = t^2$, $g' = 5t^{3/2}$. Here we set $\alpha = 0$; i.e., purely real couplings.

γ in the phase diagram at strong coupling $g' = 5t^{3/2}$. The white dots are the superconducting T_c . The color scale shows the exponent, x , with which the boson mass approaches its $T = 0$ value: $M^2(T) - M^2(T = 0) \sim T^x$. For $\gamma > \gamma_c$, the system behaves as a Fermi liquid with $x \simeq 2$ at low temperatures, while up to logarithmic corrections, we expect $x = 1$ at the QCP and within the quantum critical fan. The maximal T_c occurs just above the critical point. This figure is complementary to Fig. 2 of the main text, which shows the resistivity exponent.

We have also studied the correlation between A – the slope of the T linear resistivity – and T_c when the system is tuned precisely to the QCP at γ_c ($M = 0$). In this case T_c is tuned by varying the interaction strength g' . We find an essentially linear relationship, as may be seen in Fig. S5(a). The corresponding tuning parameter γ_c as a function of g' is shown in Fig. S5(b).

B. Full solutions to the coupled saddle point equations

Here we present the full solution to the saddle-point equations below the superconducting T_c . The momentum integrations can also be worked out analytically for the local Green's functions

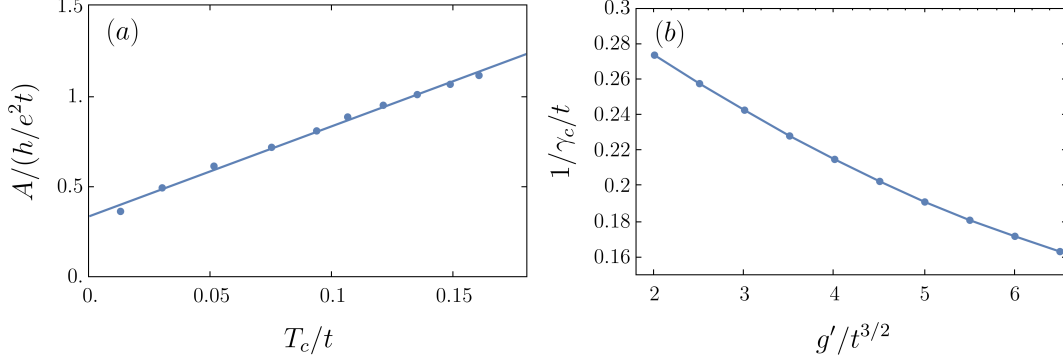


FIG. S5: (a) Relationship between slope A of the linear in T resistivity and transition temperature T_c . Here T_c is varied by varying g' while keeping the system at the QCP. (b) The (inverse) value of the tuning parameter γ at the critical point as a function of g' .

(S7a). Using the lattice dispersion (S2), we have a generalized version of (S9):

$$G_{\text{loc}}(z) = \frac{1}{2} \left(1 + \frac{zZ(z)}{\sqrt{(zZ(z))^2 - \Phi(z)^2}} \right) \frac{1}{4t} \mathcal{G} \left(\frac{-\chi(z) + \mu + \sqrt{(zZ(z))^2 - \Phi(z)^2}}{4t} \right) + \frac{1}{2} \left(1 - \frac{zZ(z)}{\sqrt{(zZ(z))^2 - \Phi(z)^2}} \right) \frac{1}{4t} \mathcal{G} \left(\frac{-\chi(z) + \mu - \sqrt{(zZ(z))^2 - \Phi(z)^2}}{4t} \right), \quad (\text{S20a})$$

$$F_{\text{loc}}(z) = \frac{\Phi(z)}{2\sqrt{(zZ(z))^2 - \Phi(z)^2}} \frac{1}{4t} \mathcal{G} \left(\frac{-\chi(z) + \mu + \sqrt{(zZ(z))^2 - \Phi(z)^2}}{4t} \right) - \frac{\Phi(z)}{2\sqrt{(zZ(z))^2 - \Phi(z)^2}} \frac{1}{4t} \mathcal{G} \left(\frac{-\chi(z) + \mu - \sqrt{(zZ(z))^2 - \Phi(z)^2}}{4t} \right). \quad (\text{S20b})$$

Here we define

$$\Sigma(z) + \Sigma(-z) \equiv 2\chi(z), \quad (\text{S21})$$

$$\Sigma(z) - \Sigma(-z) \equiv 2z(1 - Z(z)). \quad (\text{S22})$$

The Green's functions (S20) reduces to (S9) when $\Phi(z) = 0$. The analytic continuation $i\omega_n \rightarrow \omega + i0^+$ of (S20) leads to the retarded Green's functions on the real axis. Following a similar procedure to that shown in SII, we obtain the retarded self energies. The result is most compactly expressed in the real-time domain

$$\Sigma_R(t) = ig'^2(2\pi)^2\theta(t)[\tilde{A}(t)B(t) - \tilde{B}(-t)A(t)], \quad (\text{S23a})$$

$$\Phi_R(t) = -i(1 - \alpha)g'^2(2\pi)^2\theta(t)[\tilde{A}_F(t)B(t) - \tilde{B}(-t)A_F(t)], \quad (\text{S23b})$$

$$\begin{aligned} \Pi_R(t) = i2g'^2(2\pi)^2\theta(t)[\tilde{A}(t)A(-t) - \tilde{A}(-t)A(t), \\ - (1 - \alpha)(\tilde{A}_F(t)A_F(-t) - \tilde{A}_F(-t)A_F(t))]. \end{aligned} \quad (\text{S23c})$$

The self-consistent equations can also be readily solved directly on the real-axis for the retarded functions.

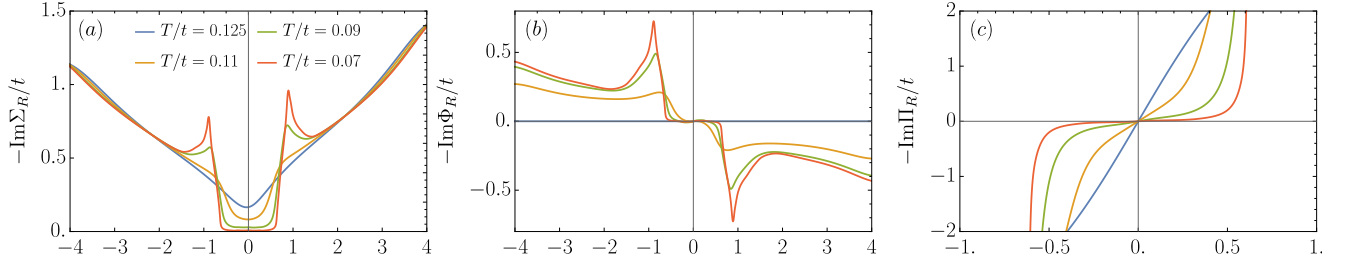


FIG. S6: (a) $-\text{Im}\Sigma_R$ at QCP ($\gamma = \gamma_c$) for different temperatures. (b) $-\text{Im}\Phi_R$ at the QCP. (c) $-\text{Im}\Pi_R$ at QCP. $-\text{Im}\Pi_R \sim \omega$ in the normal state. The coupling strength is $g' = 5t^{3/2}$.

The fermion self-energies and spectral functions are shown in Fig. 4 in the main text. In Fig. S6 we present the normal and anomalous self-energies. In Fig. S7 we report the spectral functions. The figures are all for parameters values $\mu = -0.5t$, $J = t^2$, $g' = 5t^{3/2}$, and $v = 0$.

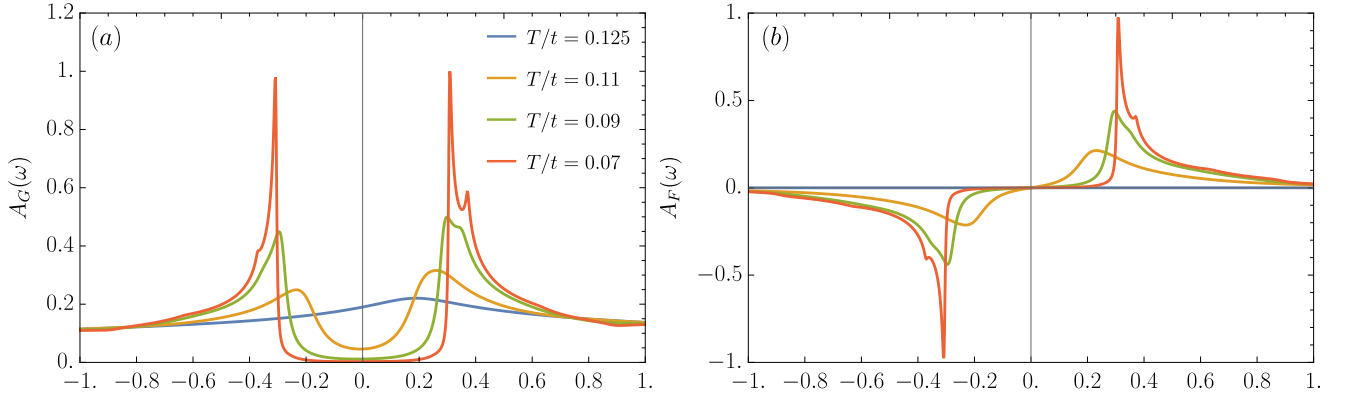


FIG. S7: Spectral functions associated to the normal (a) and anomalous (b) Green's functions. The interaction strength is $g' = 5t^{3/2}$.

SIV. CONDUCTIVITY AND SUPERFLUID STIFFNESS

The section describes our analysis of the optical conductivity and superfluid stiffness, which may be calculated after the self-consistent Green's functions have been obtained.

A. Current-current correlator

Consider the current-current correlation function $\Lambda(\mathbf{q}, \tau) = \langle T_\tau(j_\mu(\mathbf{q}, \tau)j_\nu(-\mathbf{q}, 0)) \rangle$ with

$$\begin{aligned} j_0(\mathbf{q}) &= \sum_{v_{\mathbf{k}}, \sigma} c_{\mathbf{k}, \sigma}^\dagger c_{\mathbf{k}+\mathbf{q}, \sigma} \\ \mathbf{j}(\mathbf{q}) &= \sum_{v_{\mathbf{k}}, \sigma} v_{\mathbf{k}} c_{\mathbf{k}, \sigma}^\dagger c_{\mathbf{k}+\mathbf{q}, \sigma}. \end{aligned} \quad (\text{S24})$$

Here we set the electron charge $e = 1$, but will reinstate it in the final results below. At external $\mathbf{q} = 0$, the current-current response is just the dressed bubble as seen in Figure 1:

$$\begin{aligned} \Lambda_{\alpha\beta}(i\omega_n) &= -T \sum_{n'} \int_{\mathbf{k}} v_{\mathbf{k}\alpha} v_{\mathbf{k}\beta} \left(G_{\mathbf{k}}(i\omega_{n'}) G_{\mathbf{k}}(i\omega_n + i\omega_{n'}) + F_{\mathbf{k}}^\dagger(i\omega_{n'}) F_{\mathbf{k}}(i\omega_n + i\omega_{n'}) \right) \\ &= -T \sum_{n'} \int d\epsilon \rho_{\text{tr}}^{\alpha\beta}(\epsilon) \left(G(\epsilon, i\omega_{n'}) G(\epsilon, i\omega_n + i\omega_{n'}) + F^\dagger(\epsilon, i\omega_{n'}) F(\epsilon, i\omega_n + i\omega_{n'}) \right). \end{aligned} \quad (\text{S25})$$

In the last step we introduced the ‘‘transport’’ DOS

$$\rho_{\text{tr}}^{\alpha\beta}(\epsilon) = \int_{\mathbf{k}} \frac{\partial \varepsilon_{\mathbf{k}}}{\partial k_\alpha} \frac{\partial \varepsilon_{\mathbf{k}}}{\partial k_\beta} \delta(\epsilon - \varepsilon_{\mathbf{k}}) \quad (\text{S26})$$

and used the fact that the normal and anomalous self energies are momentum independent. For the given dispersion (S2), this quantity is analytically computable

$$\rho_{\text{tr}}(\epsilon) = \frac{2t}{\pi^2} \left[E(1 - \epsilon^2/16t^2) - \frac{\epsilon^2}{16t^2} K(1 - \epsilon^2/16t^2) \right], \quad (\text{S27})$$

where E is the complete elliptic integral of the second kind. In the normal state, the analytic continuation for the retarded (R) function is

$$\Lambda_R(\omega) = \int d\epsilon \rho_{\text{tr}}(\epsilon) \int d\omega' n_F(\omega') A(\epsilon, \omega') \{ G_R(\epsilon, \omega + \omega') + [G_R(\epsilon, \omega' - \omega)]^* \}, \quad (\text{S28})$$

where n_F is the Fermi function. The final expression is efficiently evaluated via FFTs by rewriting the convolution in real-time:

$$\Lambda_R(t) = \int d\epsilon \rho_{\text{tr}}(\epsilon) \times 2\pi \{ [\tilde{A}(\epsilon, t)]^* G_R(\epsilon, t) + \tilde{A}(\epsilon, t) [G_R(\epsilon, t)]^* \}. \quad (\text{S29})$$

B. Conductivity

The conductivity is related to Λ_R according to

$$\sigma(\omega) = -\frac{\langle -K \rangle / d - \Lambda_R(\omega)}{i(\omega + i\delta)}, \quad (\text{S30})$$

where $\langle -K \rangle$ is the (negative of) the average kinetic energy per site and d is the spatial dimension (for us $d = 2$). Explicitly

$$K = -t \sum_{\langle ij \rangle, \sigma} (c_{i\sigma}^\dagger c_{j\sigma} + \text{h.c.}). \quad (\text{S31})$$

We may write

$$\sigma(\omega) = D\delta(\omega) + \sigma_{\text{reg}}(\omega) \quad (\text{S32})$$

where the Drude weight is

$$D = \pi[\langle -K/2 \rangle - \Lambda'_R(\omega \rightarrow 0)] \quad (\text{S33})$$

and

$$\sigma_{\text{reg}}(\omega) = \frac{\Lambda''_R(\omega)}{\omega} - i \frac{\Lambda'_R(\omega) - \langle -K/2 \rangle}{\omega}. \quad (\text{S34})$$

In a disordered system, the δ -function contribution vanishes (there is a finite dc resistance), from which we find

$$D = 0 \Rightarrow \langle -K/2 \rangle = \Lambda'_R(\omega \rightarrow 0) \quad (\text{S35})$$

and we may also write

$$\sigma(\omega) = \frac{\Lambda''_R(\omega)}{\omega} - i \frac{\Lambda'_R(\omega) - \Lambda'_R(\omega \rightarrow 0)}{\omega} \quad (\text{disordered system}). \quad (\text{S36})$$

This form is useful since it does not require computing independently $\langle K \rangle$ (although explicitly comparing the left- and right-hand sides of Eq. (S35) is a useful consistency check). Another useful result that follows from Kramers-Kronig is the sum rule

$$\int_{-\infty}^{\infty} d\omega \sigma(\omega) = \pi \langle -K/2 \rangle. \quad (\text{S37})$$

Finally, note the dc limit for the conductivity can also be taken explicitly:

$$\sigma_{\text{dc}} = \lim_{\omega \rightarrow 0} \frac{\Lambda''_R(\omega)}{\omega} = \pi \int d\epsilon \rho_{\text{tr}}(\epsilon) \int d\omega' \left(-\frac{\partial n_F}{\partial \omega'} \right) [A(\epsilon, \omega')]^2. \quad (\text{S38})$$

As described in the main text, we have parametrized the conductivity in the form [6]

$$\sigma(\omega) = i \frac{e^2 K/2}{\omega \frac{m^*(\omega)}{m} + \frac{i}{\tau_{\text{tr}}(\omega)}}, \quad (\text{S39})$$

and so determine a frequency dependent effective mass enhancement $m^*(\omega)/m$ and transport scattering time $\tau_{\text{tr}}(\omega)$. We show the results in Figs. S8. We also show results for the absolute value and phase of the complex conductivity in Fig. S8 (e-f), with results which are very similar to the corresponding results of Michon *et al.* [6].

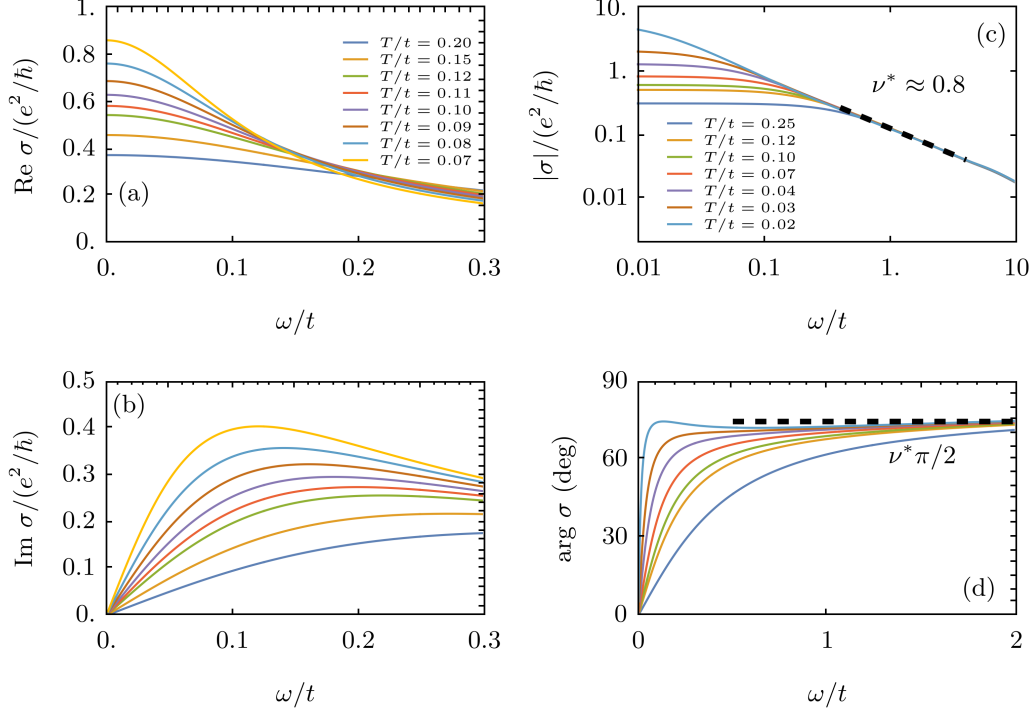


FIG. S8: Optical conductivity at larger coupling $g' = 5t^{3/2}$ and $\nu = 0$. (a,b) Normal state optical conductivity at the quantum critical coupling for various temperatures indicated in Panel (a). (c,d) Modulus and phase of $\sigma(\omega)$ with temperatures indicated in Panel (c).

Another way to extract the transport scattering time is motivated from the Drude formula:

$$\sigma'_{\text{Drude}}(\omega) = \sigma_{\text{dc}} \frac{1}{1 + (\omega\tilde{\tau}_{\text{tr}})^2} \quad (\text{S40})$$

This motivates the identification more generally:

$$\frac{\sigma_{\text{dc}}}{\sigma'(\omega)} - 1 = (\omega\tilde{\tau}_{\text{tr}})^2 + \dots \quad (\text{S41})$$

where \dots denote terms higher order in ω . From the fits we may extract $\tilde{\tau}_{\text{tr}}$ from Eq. (S41): Writing $\tilde{\tau}_{\text{tr}}^{-1} = \alpha T$ we see that (1) α is a function of T for $T \lesssim 0.1t$ and (2) for $T \gtrsim 0.1t$ we have $\alpha \simeq 0.4$.

C. Superfluid stiffness

The coefficient D of the delta function, the Drude weight, can be obtained by extrapolating $i\omega_n \rightarrow 0$ [7]. If there is a gap, $D = \rho_s$, and the superfluid stiffness is

$$\frac{\rho_s}{\pi e^2} = \langle -K \rangle / 2 - \Lambda(i\omega_n = 0), \quad (d = 2). \quad (\text{S42})$$

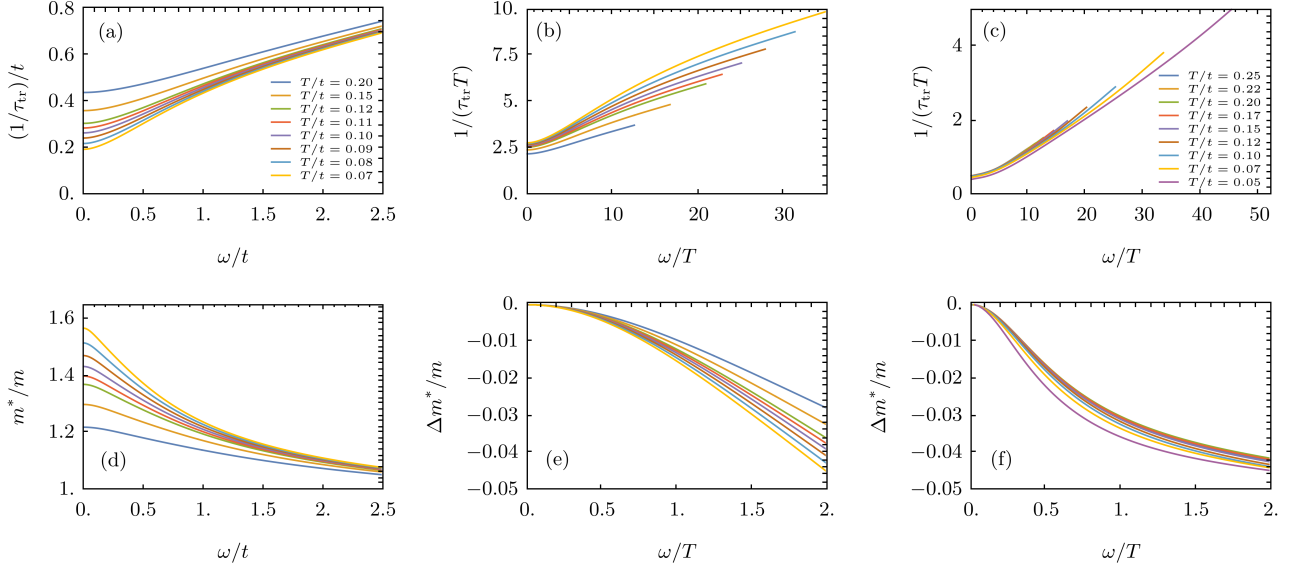


FIG. S9: (a,d) Transport scattering rate $1/\tau_{\text{tr}}$ and effective mass m^* obtained from σ using (3) at larger coupling $g' = 5t^{3/2}$. (b) A scaling plot with $1/\tau_{\text{tr}}$ and ω scaled by T at $g' = 5t^{3/2}$. (c) Same as (b) at $g' = 2t^{3/2}$. (e) A scaling plotting showing $\Delta m^*/m = m^*(\omega)/m - m^*(0)/m$ as a function of ω/T at $g' = 5t^{3/2}$. (f) Same as (e) at $g' = 2t^{3/2}$.

The two weighted densities of states $\rho_{\text{tr}}(\epsilon) \equiv \frac{1}{N} \sum_k v_k^2 \delta(\epsilon - \epsilon_k)$ and $\rho_0(\epsilon) \equiv \frac{1}{N} \sum_k \delta(\epsilon - \epsilon_k)$ are closely related with each other

$$\frac{d\rho_{\text{tr}}(\epsilon)}{d\epsilon} = -\frac{\epsilon}{2}\rho_0(\epsilon). \quad (\text{S43})$$

Therefore, we can rewrite the average kinetic energy per site as

$$\begin{aligned} \langle K \rangle &= \frac{1}{\beta} \sum_{\omega_n} \frac{1}{N} \sum_k \epsilon_k G(k, i\omega_n) e^{i\omega_n 0^+} = \frac{1}{\beta} \sum_{\omega_n} \int d\epsilon \rho_0(\epsilon) \epsilon G(\epsilon, i\omega_n) e^{i\omega_n 0^+} \\ &= -\frac{2}{\beta} \sum_{\omega_n} \int d\epsilon \frac{d\rho_{\text{tr}}(\epsilon)}{d\epsilon} G(\epsilon, i\omega_n) e^{i\omega_n 0^+} = \frac{2}{\beta} \sum_{\omega_n} \int d\epsilon \rho_{\text{tr}}(\epsilon) \frac{dG(\epsilon, i\omega_n)}{d\epsilon} e^{i\omega_n 0^+} \end{aligned} \quad (\text{S44})$$

From Dyson's equation,

$$\frac{\partial G(\epsilon, i\omega_n)}{\partial \epsilon} = G(\epsilon, i\omega_n)^2 - F^\dagger(\epsilon, i\omega_n) F(\epsilon, i\omega_n), \quad (\text{S45})$$

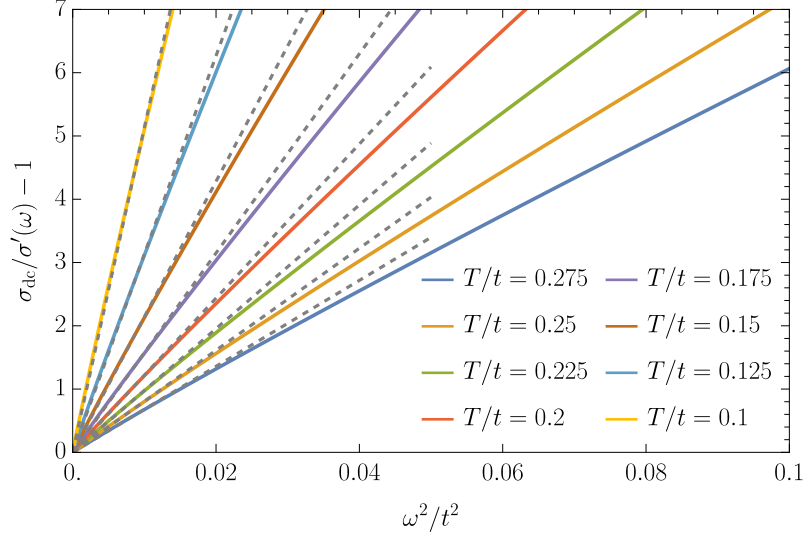


FIG. S10: Linear fits of $\sigma_{dc}/\sigma'(\omega) - 1$ vs ω^2 for different temperatures. The gray, dashed lines corresponding to linear fits.

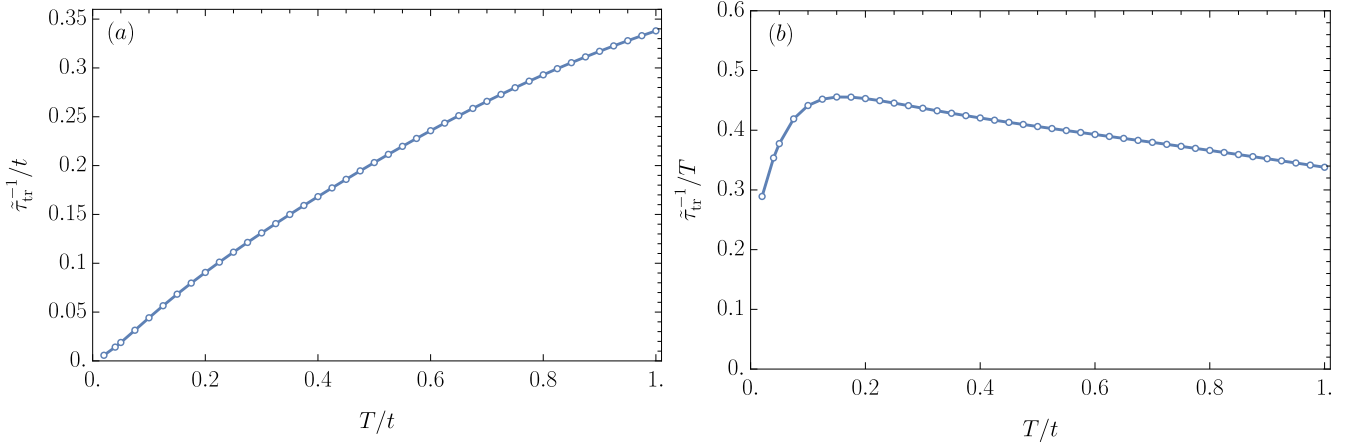


FIG. S11: (a) Transport scattering rate $1/\tilde{\tau}_{tr}$ extracted from linear fits of $\sigma_{dc}/\sigma'(\omega) - 1$. (b) A scaling plot with $1/\tilde{\tau}_{tr}$ scaled by T .

and we get for the superfluid stiffness

$$\begin{aligned}
\frac{\rho_s}{\pi e^2} &= \langle -K/2 \rangle - \Lambda(0) \\
&= -T \sum_n \int d\epsilon \rho_{\text{tr}}(\epsilon) (G(\epsilon, i\omega_n)^2 - F^\dagger(\epsilon, i\omega_n) F(\epsilon, i\omega_n)) \\
&\quad + T \sum_n \int d\epsilon \rho_{\text{tr}}(\epsilon) (G(\epsilon, i\omega_n)^2 + F^\dagger(\epsilon, i\omega_n) F(\epsilon, i\omega_n)) \\
&= 2T \sum_n \int d\epsilon \rho_{\text{tr}}(\epsilon) F^\dagger(\epsilon, i\omega_n) F(\epsilon, i\omega_n).
\end{aligned} \tag{S46}$$

SV. HOMES' LAW

Here we describe the relation between Homes law [8] and our data. To begin, we convert the results of Homes *et al.* [8] to dimensionless units. We use S.I. units throughout for fundamental constants.

Let Σ be the value of the conductivity in $\text{Ohm}^{-1} \text{ cm}^{-1}$. Then the conductivity, σ , is

$$\sigma = 100\Sigma \text{ Ohm}^{-1} \text{ meter}^{-1} \tag{S47}$$

Let R be the value of the superfluid density in cm^{-2} , as quoted in Ref. [8]. Then the associated plasma frequency ω_p is

$$\omega_p^2 = (100 \times 2\pi c)^2 R \text{ sec}^{-2} \tag{S48}$$

This is connected to our definition of the superfluid density, ρ_s :

$$\begin{aligned}
\sigma(\omega) &= i \frac{\rho_s}{\hbar\omega} \\
\varepsilon(\omega) &= \varepsilon_0 + \frac{i\sigma(\omega)}{\omega} = -\varepsilon_0 \frac{\omega_p^2}{\omega^2} \text{ as } \omega \rightarrow 0 \\
\Rightarrow \rho_s &= \hbar\varepsilon_0\omega_p^2
\end{aligned} \tag{S49}$$

So for the dimensionless ratio expressing Homes' Law, we have

$$\begin{aligned}
\frac{\rho_s}{\sigma k_B T_c} &= \frac{\hbar\varepsilon_0(200\pi c)^2 R}{100k_B \Sigma T_c} \\
&= 0.024 \frac{R}{\Sigma T_c} \\
&\simeq 2.88,
\end{aligned} \tag{S50}$$

where in the last line we used the value $R/(\Sigma T_c) \simeq 120$ obtained in Ref. [8].

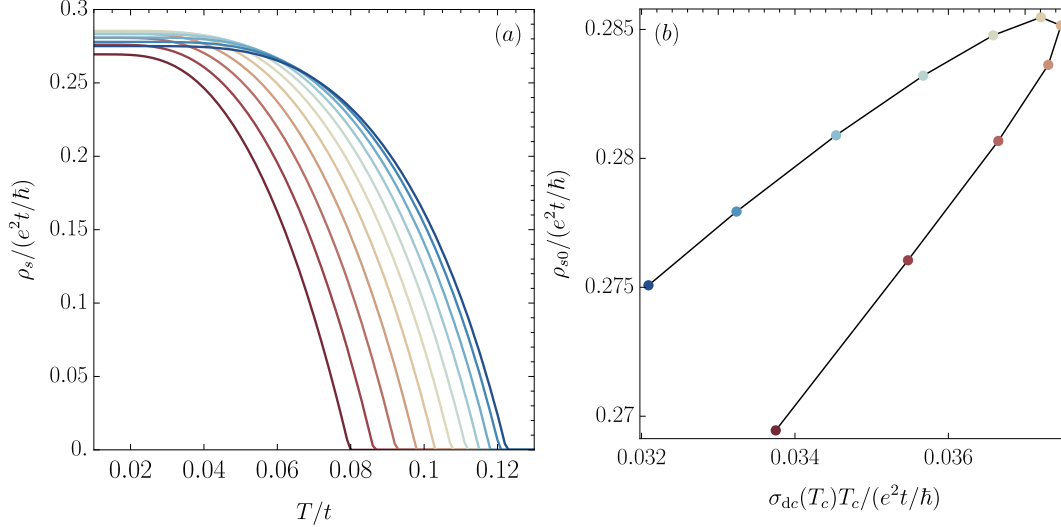


FIG. S12: (a). Temperature dependence of superfluid stiffness ρ_s at $g' = 5t^{3/2}$, $v = 0.6$ for various values of renormalized boson mass M . (b). The plot of zero temperature superfluid density ρ_{s0} vs $\sigma_{dc}T_c$ in the unit of e^2t/\hbar ; the best fit value of the slope for the 5 points closest to the QCP is 2.17.

We show a plot of the superfluid density ρ_s as a function of T for various values of distance from the QCP in Figs. 5 and S12. When $v = 0$, we find a decreasing T_c is accompanied by an increasing ρ_{s0} , the superfluid stiffness at $T = 0$, as in Fig. 5. On the other hand, when v is non-zero, we find that with decreasing T_c , the stiffness initially increases, and then decreases, as shown in Fig. S12a. For $v = 0.75$, the ratio $\rho_{s0}/(\sigma_{dc}(T_c)T_c)$ takes a value close to (S50), as shown in Fig. S12b.

-
- [1] D. Hauck, M. J. Klug, I. Esterlis, and J. Schmalian, *Eliashberg equations for an electron–phonon version of the Sachdev–Ye–Kitaev model: Pair breaking in non-Fermi liquid superconductors*, [Annals of Physics](#) **417**, 168120 (2020).
 - [2] I. Esterlis, H. Guo, A. A. Patel, and S. Sachdev, *Large N theory of critical Fermi surfaces*, [Phys. Rev. B](#) **103**, 235129 (2021), [arXiv:2103.08615 \[cond-mat.str-el\]](#).
 - [3] I. Esterlis and J. Schmalian, *Cooper pairing of incoherent electrons: an electron-phonon version of the Sachdev-Ye-Kitaev model*, [Phys. Rev. B](#) **100**, 115132 (2019), [arXiv:1906.04747 \[cond-mat.str-el\]](#).
 - [4] P. M. Dee, K. Nakatsukasa, Y. Wang, and S. Johnston, *Temperature-filling phase diagram of the two-dimensional Holstein model in the thermodynamic limit by self-consistent Migdal approximation*, [Phys. Rev. B](#) **99**, 024514 (2019).
 - [5] J. Schmalian, M. Langer, S. Grabowski, and K. Bennemann, *Self-consistent summation of many-*

- particle diagrams on the real frequency axis and its application to the flex approximation*, Computer physics communications **93**, 141 (1996).
- [6] B. Michon, C. Berthod, C. W. Rischau, A. Ataei, L. Chen, S. Komiya, S. Ono, L. Taillefer, D. van der Marel, and A. Georges, *Reconciling scaling of the optical conductivity of cuprate superconductors with Planckian resistivity and specific heat*, [Nature Communications](#) **14**, 3033 (2023), [arXiv:2205.04030 \[cond-mat.str-el\]](#).
- [7] D. J. Scalapino, S. R. White, and S. Zhang, *Insulator, metal, or superconductor: The criteria*, [Phys. Rev. B](#) **47**, 7995 (1993).
- [8] C. C. Homes, S. V. Dordevic, M. Strongin, D. A. Bonn, R. Liang, W. N. Hardy, S. Komiya, Y. Ando, G. Yu, N. Kaneko, X. Zhao, M. Greven, D. N. Basov, and T. Timusk, *A universal scaling relation in high-temperature superconductors*, [Nature \(London\)](#) **430**, 539 (2004), [arXiv:cond-mat/0404216 \[cond-mat.supr-con\]](#).